Unidirectional Spin Hall Magnetoresistance in Antiferromagnetic Heterostructures

Yang Cheng, Junyu Tang, Justin J. Michel, Su Kong Chong, Fengyuan Yang, Ran Cheng, and Kang L. Wang

Unidirectional Spin Hall Magnetoresistance in Antiferromagnetic Heterostructures

Yang Cheng[1,*], Junyu Tang[2], Justin J. Michel[3], Su Kong Chong[1], Fengyuan Yang[3], Ran Cheng[2,4], and Kang L. Wang[1,*]

[1]*Department of Electrical and Computer Engineering, and Department of Physics and Astronomy, University of California, Los Angeles, CA 90095, USA*

[2] *Department of Physics and Astronomy, University of California, Riverside, CA 92521, USA*

[3]*Department of Physics, The Ohio State University, Columbus, OH 43210, USA*

[4] *Department of Electrical and Computer Engineering, University of California, Riverside, CA 92521, USA*

Corresponding author. E-mail: [*]cheng991@g.ucla.edu, [*]wang@ee.ucla.edu

Abstract

Unidirectional spin Hall magnetoresistance (USMR) has been widely reported in the heavy metal / ferromagnet (HM/FM) bilayer systems. We observe the USMR in Pt/α-Fe$_2$O$_3$ bilayers where the α-Fe$_2$O$_3$ is an antiferromagnetic (AFM) insulator. Systematic field and temperature dependent measurements confirm the magnonic origin of the USMR. The appearance of AFM-USMR is driven by the imbalance of creation and annihilation of AFM magnons by spin orbit torque due to the thermal random field. However, unlike its ferromagnetic counterpart, theoretical modeling reveals that the USMR in Pt/α-Fe$_2$O$_3$ is determined by the antiferromagtic magnon number with a non-monotonic field dependence. Our findings extend the generality of the USMR which pave the ways for the highly sensitive detection of AF spin state.

The detection of the spin state is one of the central topics in spintronics[1-3]. Spin Hall magnetoresistance (SMR) has been widely used to probe magnetization in heavy meatal/ (anti)ferromagnetic (HM/(A)FM) heterostructures[2,4-7]. When the current is applied in a heavy metal layer, the generated spin current is injected to the adjacent magnetic layer. The additional currents induced by inverse spin Hall effects change the resistivity of the heterostructures where its magnitude only depends on the relative angle between magnetization and spin polarization. So far, SMR has been widely reported in both ferromagnetic and antiferromagnetic systems. Recently, a new type of magnetoresistance --- unidirectional SMR (USMR)[8-11] --- has attracted intense interest. Compared with conventional SMR, the USMR is a non-linear magnetoresistance where the measured voltage depends quadratically on the applied current. What's more, the magnitude unidirectionally depends on the angle between spin polarization and magnetization as its name suggests, which provides a more precise way to probe the spin state in the magnetic layer. USMR has been observed only in HM/FM heterostructures. For metallic FM, the USMR is originated from either spin-dependent electron scattering (spin-dependent USMR) or electron-magnon scattering (spin-flip USMR) [9,12]. For insulating FM, for example $Pt/Y_3Fe_5O_{12}$ (YIG) bilayers[10], the observed USMR is attributed to the imbalance of magnon generation and annihilation rate by the spin-orbit torque. Although the SMR has been observed in both FMs and AFMs, the USMR is not expected in the AFMs. Even for YIG which is a ferrimagnet, the observed USMR behaves like a ferromagnet, but is not related to its antiferromagnetic ordering [13]. This is because the order parameter of AFMs, the staggered magnetization (Néel vector), is a pair of two sublattice magnetizations, which makes the spin polarization with a 180º rotational symmetry relative to the Néel vector. A possible way to break this symmetry is by applying an external field to induce a net FM order from sublattice magnetization canting. Here, we report the detection of USMR in Pt/α-Fe_2O_3 bilayers using the second harmonic measurements. Through systematic field and temperature dependent measurement, and theoretical modeling, we attribute the observed USMR to the imbalance of the magnon generation and

annihilation rates, similar to the USMR in FM insulators [10]. However, the antiferromagnetic magnon plays a dominant role whereas the induced magnetization only contributes a small part to the USMR from our simulation.

α-Fe$_2$O$_3$ is an easy-plane antiferromagnet with the Néel temperature around 953 K [14]. The weak anisotropy field of three easy-axes in the *ab*-plane (0001) makes the spin-flop (or spin reorientation) occur at the critical field of ~ 1T, where the Néel order is perpendicular to the magnetic field, $\boldsymbol{n} \perp \boldsymbol{H}$ [15]. This makes the field control of the Néel order of α-Fe$_2$O$_3$ much easier compared with most of typical antiferromagnets, a necessary condition for the extraction of the USMR. We grow a Pt (5nm)/ α-Fe$_2$O$_3$ (30 nm) thin film stack on Al$_2$O$_3$ (0001) using off-axis magnetron sputtering [15]. Bulk α-Fe$_2$O$_3$ experiences the so-called Morin transition, which changes its phase from easy-plane AFM to easy-axis (c-axis [0001]) AFM at ~ 260K. However, due to the strain induced enhancement of hard-axis anisotropy, our thin film α-Fe$_2$O$_3$ does not show such transition down to 10 K as had been demonstrated in our previous research[15-18]. After the growth the of Pt/α-Fe$_2$O$_3$ bilayer, we pattern our sample into a Hall bar device with a length (l) 10 µm and a width (w) 5 µm, as shown in Fig. 1(a).

Since USMR is a non-linear current effect, an angular dependent harmonic measurement method is commonly used [10,19]. For the harmonic measurement setup, a low frequency 5 Hz ac current $I = I_0\sin(\omega t)$ is applied to the Hall bar device. The longitudinal (V_{xx}) and transverse (V_{xy}) voltage are measured simultaneously under an in-plane magnetic field. The first harmonic response is the same as the DC measurement, where [20]

$$V_{xx}{}^{1\omega} = V_{\mathrm{SMR}}\sin^2\varphi_{\mathrm{H}} \tag{1}$$

$$V_{xy}{}^{1\omega} = -V_{\mathrm{TSMR}}\sin\varphi_{\mathrm{H}}\cos\varphi_{\mathrm{H}}. \tag{2}$$

Here φ_{H} is the in-plane angle between applied field and current direction, as shown in Fig 1(a). V_{SMR} and V_{TSMR} are the longitudinal and transverse spin Hall magnetoresistance where $\frac{V_{\mathrm{SMR}}}{V_{\mathrm{TSMR}}} = \frac{l}{w} = 2$, the aspect ratio of our Hall bar [15,21]. Figure 1(b) shows the angular dependent first harmonic measurement at 2

T and 300 K. The current $I_0 = 6$ mA. Figure 1(c) shows the extracted V_{SMR} and V_{TSMR} using Eq. (1) and (2) as the field increases from 0.3 T to 9 T. The magnitude of V_{SMR} and V_{TSMR} saturates near 1 T, which indicates a single domain AFM state at $\mu_0 H > 1$ T. The ratio of V_{SMR} and V_{TSMR} is shown in the inset of Fig. 1(c), which is close to 2, as expected.

As shown in Fig. 2(a), a current induced effect such as spin-orbit torque drives the Néel order away from its equilibrium position where the change of magnetoresistance can be probed via the second harmonic voltage $V_{xx}{}^{2\omega}$ and $V_{xy}{}^{2\omega}$. Based on our previous research [20] [for more details, see Supplementary Materials (SM)], the second harmonic voltage can be rewritten as

$$V_{xx}{}^{2\omega} = V_{xx,\text{FL}}{}^{2\omega} + V_{xx,\text{SSE}}{}^{2\omega} + V_{xx,\text{USMR}}{}^{2\omega}$$

$$= -\frac{1}{2}V_{\text{SMR}}\frac{H_{\text{FL}}}{H}\sin(2\varphi_{\text{H}})\cos\varphi_{\text{H}} - (V_{xx,\text{SSE}} + V_{xx,\text{USMR}})\sin\varphi_{\text{H}} \tag{3}$$

$$V_{xy}{}^{2\omega} = V_{xy,\text{FL}}{}^{2\omega} + V_{xy,\text{SSE}}{}^{2\omega}$$

$$= \frac{1}{2}V_{\text{TSMR}}\frac{H_{\text{FL}}}{H}\cos(2\varphi_{\text{H}})\cos\varphi_{\text{H}} + V_{xy,\text{SSE}}\cos\varphi_{\text{H}}. \tag{4}$$

Here, H_{FL} is the field-like torque effective field. The longitudinal $V_{xx,\text{FL}}{}^{2\omega}$, $V_{xx,\text{SSE}}{}^{2\omega}$, and $V_{xx,\text{USMR}}{}^{2\omega}$ are the contributions from field-like torque, spin Seebeck effect, and USMR, respectively. The transverse $V_{xy,\text{FL}}{}^{2\omega}$ and $V_{xy,\text{SSE}}{}^{2\omega}$ are the field-like torque and spin Seebeck effect terms. Notice that USMR only shows up in the $V_{xx}{}^{2\omega}$ term. To extract the USMR contributions $V_{xx,\text{USMR}}$, we first fit the $V_{xx}{}^{2\omega}$ and $V_{xy}{}^{2\omega}$ to get the $V_{xx,\text{SSE}} + V_{xx,\text{USMR}}$ and $V_{xy,\text{SSE}}$; $V_{xx,\text{USMR}}$ can be separated from $V_{xx,\text{SSE}}$ given that $\frac{V_{xx,\text{SSE}}{}^{2\omega}}{V_{xy,\text{SSE}}{}^{2\omega}} = \frac{l}{w} = 2$. Compared with the fitting to ferromagnets, the transverse second harmonic voltage does not contain the damping-like (DL) torque term, which makes the results more convincing due to less fitting process [10]. Figure 2 (b) and (c) shows the angular dependence of second harmonic voltage $V_{xx}{}^{2\omega}$ and $V_{xy}{}^{2\omega}$ at 2 T and 300 K. We fit the data using Eq. (3) and (4). Clearly, there is a USMR contribution in $V_{xx}{}^{2\omega}$ after subtracting the longitudinal spin Seebeck component $V_{xx,\text{SSE}}{}^{2\omega}$ with the same angular dependence.

4

Following the same process, we obtain $V_{xx}{}^{2\omega}$ and $V_{xy}{}^{2\omega}$ of the Pt(5 nm)/ α-Fe$_2$O$_3$ (30 nm) bilayer

from 1 T to 9 T and fitting curves, as shown in Fig. 3(a) and (b). Figure 3 (c) shows the fitted field-like

torque component from Fig. 3(a) and (b). The extracted $V_{xx,\text{FL}}{}^{2\omega}$ and $V_{xy,\text{FL}}{}^{2\omega}$ decrease with the

increasing field and follows a 1/H dependence. The ratio of $V_{xx,\text{FL}}{}^{2\omega}$ and $V_{xy,\text{FL}}{}^{2\omega}$ is shown in the blue

curve of Fig. 3(e), which is around 2 for the entire field range as $\frac{V_{xx,\text{FL}}{}^{2\omega}}{V_{xy,\text{FL}}{}^{2\omega}} = \frac{V_{\text{SMR}}}{V_{\text{TSMR}}} = \frac{l}{w} = 2$. At the same

time, the sinusoidal and cosinusoidal components in $V_{xx}{}^{2\omega}$ and $V_{xy}{}^{2\omega}$ are extracted by fitting the data

with Eq. (3) and (4) where the ratio of them are plotted in the green curve of Fig. 3(e). The sinusoidal term

in $V_{xx}{}^{2\omega}$ is expected to contain both longitudinal spin Seebeck and USMR contributions while the

cosinusoidal term in $V_{xy}{}^{2\omega}$ is only from the transverse spin Seebeck voltage, which is linearly proportional

to the field H since $V_{\text{SSE}}{}^{2\omega} \propto \boldsymbol{m} \propto H$[22]. In the green curve of Fig. 3(e), it is shown that the ratio of

$\frac{V_{xx,\text{SSE}}{}^{2\omega} + V_{xx,\text{USMR}}{}^{2\omega}}{V_{xy,\text{SSE}}{}^{2\omega}} > 2$, indicating the existence of USMR.

Figure 4(a) shows the field dependence of extracted USMR at 300 K. Surprisingly, unlike the USMR

in a ferromagnet where the magnitude either monotonically decreases or is unchanged as the field

increases, the USMR in the antiferromagnetic Pt/α-Fe$_2$O$_3$ bilayer shows a non-monotonic field

dependence. The magnitude of USMR increases and reaches maximum at 2 T and then decreases and

approaches zero. Since the AFM α-Fe$_2$O$_3$ is an insulator, this excludes the possibility of spin-dependent or

spin-flip mechanisms that require electron spin carriers. Recently, magnonic USMR has been observed in

the insulating ferromagnetic bilayer Pt/YIG [10]. To testify the role played by magnons in the observed

USMR, we perform the temperature dependent measurement as shown in Fig. 4(b). When the applied

field is 2 T and the temperature decreases from 325 K, the USMR monotonically drops. At and below 200

K, no USMR is observed. This temperature dependence measurement provides the strong evidence for

the magnonic origin of USMR [9].

Following the theory of magnon creation and annihilation imbalance in ferromagnet, we extend

it to the antiferromagnetic regime. The coupled Landau–Lifshitz–Gilbert (LLG) equations for two sublattice magnetic moments $\boldsymbol{m_A}$ and $\boldsymbol{m_B}$ are written as [23]

$$\dot{\boldsymbol{m}}_A = -\gamma \boldsymbol{m_A} \times \boldsymbol{H}_A^{eff} - \gamma J_{\text{ex}} \boldsymbol{m_A} \times \boldsymbol{m_B} + \alpha \boldsymbol{m_A} \times \dot{\boldsymbol{m}}_A + \gamma \boldsymbol{\tau}_\mathbf{A}^{\mathbf{DL}}, \qquad (7)$$

$$\dot{\boldsymbol{m}}_B = -\gamma \boldsymbol{m_B} \times \boldsymbol{H}_B^{eff} - \gamma J_{\text{ex}} \boldsymbol{m_B} \times \boldsymbol{m_A} + \alpha \boldsymbol{m_B} \times \dot{\boldsymbol{m}}_B + \gamma \boldsymbol{\tau}_\mathbf{B}^{\mathbf{DL}}, \qquad (8)$$

where the effective field $\boldsymbol{H}_{A(B)}^{eff} = \boldsymbol{H_0} + \boldsymbol{h}_{\mathbf{A(B)}} + \boldsymbol{H}_{A(B)}^{DMI} + \boldsymbol{H}_{A(B)}^{hard}$ contains the external magnetic field $\boldsymbol{H_0}$, the thermal random field $\boldsymbol{h}_{\mathbf{A(B)}}(T)$, the effective field induced by Dzyaloshinskii–Moriya interaction (DMI) $\boldsymbol{H}_{A(B)}^{DMI} = H_D\big(\pm \boldsymbol{m}_{B(A)} \times \hat{\boldsymbol{z}}\big)$ [24] and effective field of the hard axis anisotropy $\boldsymbol{H}_{A(B)}^{hard} = 2H_\perp m_{A(B)}^z \hat{\boldsymbol{z}}$. $J_{\text{ex}}(< 0)$ is the AFM exchange coupling, γ is the gyromagnetic ratio (positive), and α is the Gilbert damping constant. $\boldsymbol{\tau}_{\mathbf{A(B)}}^{\mathbf{DL}} = H_{\text{DL}} \boldsymbol{m}_{\mathbf{A(B)}} \times (\hat{\boldsymbol{\sigma}} \times \boldsymbol{m}_{\mathbf{A(B)}})$ is the damping-like (DL) torque that exerts on the unit sublattice magnetization $\boldsymbol{m}_{\mathbf{A(B)}}$, as shown in Fig.2(a). Here, $\hat{\boldsymbol{\sigma}}$ is the unit vector (along $\hat{\boldsymbol{y}}$ axis) of the spin polarization induced by the spin Hall effect in Pt with amplitude H_{DL} being linearly proportional to the charge current density. In our previous work, we have demonstrated that without the thermal random field, the DL torque induced a rotation of the sublattice magnetization (as well as the net magnetization $\boldsymbol{m}$ and Néel vector $\boldsymbol{n}$) $\Delta\varphi_{\mathbf{A(B)}} = \Delta\varphi_{\boldsymbol{m}} = \Delta\varphi_{\boldsymbol{n}} \propto H_{\text{DL}}^2 \propto I^2$ [20]. Therefore, the induced voltage change $\propto I^3$, which cannot be detected in the second harmonic signal $V^{2\omega}$ but rather in third harmonic voltage $V^{3\omega}$, and it is not unidirectional. However, after considering the thermal random field $\boldsymbol{h}_{\mathbf{A(B)}}(T)$, the damping-like torque induces a fluctuation of the sublattice magnetizations, which is now linear to the I, and unidirectional. The longitudinal SMR for a Pt/AFM insulator heterostructure can be presented as $\rho_L = \rho_0 - \Delta\rho\langle n_y^2 \rangle$ [5,6,21], where the contribution from net magnetization $-\Delta\rho\langle m_y^2 \rangle$ is negligible in the AFM regime. When an external magnetic field or applied current is reversed, the asymmetric magnon excitation driven by the thermal random field will result in a USMR in ρ_L [10]. For a current applied along

6

the $\hat{x}$ direction, the USMR signal reaches the maximum (minimum) at $\varphi_H = \pm\frac{\pi}{2}$ ($\pm\pi$) [Fig. 2(a)]. This can

be explained by the fact that the induced net FM order is aligned along the external field $\boldsymbol{H}$ ($\varphi_H = \varphi_M$).

Therefore, $\boldsymbol{H}$ aligned along $\pm\hat{y}$ are inequivalent for magnon excitation when the spin polarization $\boldsymbol{\sigma}$ lies

at $+\hat{y}$. However, when $\boldsymbol{H}$ is reversed between $\pm\hat{x}$, there is no asymmetry in magnon excitation. The

USMR amplitude and antiferromagnetic magnon number difference are both proportional to the

difference $\langle n_y^2 \rangle_+ - \langle n_y^2 \rangle_-$ ($\pm$ sign indicates two opposite directions). In the following, we refer the term

$\langle n_y^2 \rangle_+ - \langle n_y^2 \rangle_-$ as "antiferromagnetic magnon number difference" for convenience since the trivial

proportionality does not affect the physical picture[10]. We then numerically calculate the field

dependence of antiferromagnetic magnon number difference for $\varphi_H = \pm\frac{\pi}{2}$ (see Section 1 in SM for more

details [26]). We find that the field dependence of antiferromagnetic magnon number difference

qualitatively agrees with the non-monotonic trend of the USMR signal and the peak around 2T [Fig. 4(a)]

is reproduced [Fig. 5(a)]. We also calculate the antiferromagnetic magnon number difference between

$\varphi_H = 0, \pi$ in Fig. 5(b). As expected, we find that $\langle n_y^2 (\varphi_H = 0) \rangle - \langle n_y^2 (\varphi_H = \pi) \rangle = 0$, which is

consistent with the results from Fig. 2(a). The decrease of USMR at high fields is due to the suppression

of magnon excitations at large $\boldsymbol{H_0}$, which is similar to the Pt/FM case. However, unlike FM where the

magnetization simply saturates at small fields ($\boldsymbol{m} \parallel \boldsymbol{H_0}$), the external field can increase the canting of

sublattice magnetization in AFM ($\boldsymbol{n} \perp \boldsymbol{H_0}$). Therefore, the magnetic fluctuation is governed by $\boldsymbol{H_0}$ in a

more complicated way. Specifically, the canting angle $\Delta\varphi$ for sublattice magnetizations of α-Fe_2O_3

depends on H_D, J_{ex} and H_0 as $\Delta\varphi = -\arcsin((H_0 + H_D)/2J_{ex})$. With the thermal random field $\boldsymbol{h}$ acting

on the two orthogonal $\hat{e}_\varphi$ and $\hat{e}_r$ directions, the dynamical magnetic susceptibility χ that characterizes

the fluctuation of Néel vector $\Delta\boldsymbol{n_y} = \chi \cdot \boldsymbol{h}$ contains a highly nontrivial H_0 dependence through $\Delta\varphi$,

leading to the non-monotonic field dependence of USMR in AFM. In Fig. S1(a) (See SM for details), we

manually eliminate the H_0 dependence of $\Delta\varphi$ and plot the field dependence of magnon number

difference. We find that the peak around 2 T disappears and the field dependence returns to be

monotonic which is similar to the Pt/FM case. Therefore, the field-assisted canting, which is unique in AFM, increases the imbalance in the creation and annihilation of AFM magnons. However, on the other hand, total magnon number is suppressed with increasing field and the magnon excitation is essentially frozen when the field is large enough. These two competing effects give rise to the non-monotonic field dependence of magnonic USMR. Finally, we compare the contributions with those of ferromagnetic magnon $\langle m_y^2 \rangle_+ - \langle m_y^2 \rangle_-$ as shown in Fig. S1(b), which is three orders of magnitude smaller than that of antiferromagtic magnons, emphasizing the dominate role of antiferromagnetic magnons in the observed USMR.

In summary, we observe the USMR in the antiferromagnetic heterostructure in Pt/ α-Fe$_2$O$_3$ bilayers. The magnonic origin of USMR is revealed in the temperature and field dependent measurements. It is shown that the antiferromagnetic magnon plays the dominant role which gives a unique field dependence as compared with that of ferromagnetic materials. This first evidence of USMR in HM/AFI bilayers significantly expands our materials base to include the large family of AF insulators and paves the way for the highly sensitive detection of AF spin state in emerging the AF spintronics through USMR.

Note added: Recently we became aware of an independent report [25] which detected UMR in metallic AFM bilayer Pt/FeRh. the UMR observed in Pt/FeRh is originated from the Rashba SOC at metal/AFM interface. Compared with the USMR observed in this work which only has the longitudinal term where Rashba type UMR should also have the corresponding transverse component with the magnitude $\frac{V_{xx,\text{Rashba UMR}}^{2\omega}}{V_{xy,\text{Rahsba UMR}}^{2\omega}} = \frac{l}{w}$. Thus, the Rashba SOC induced UMR could be mixed with the spin Seebeck signal in our analysis. Compared with metallic bilayers with almost no thermal effects due to a negligible temperature gradient, the spin Seebeck effect is very likely to overwhelm the Rashba UMR in our insulating α-Fe$_2$O$_3$ bilayers.

Reference

[1]   S. Ikeda, J. Hayakawa, Y. Ashizawa, Y. M. Lee, K. Miura, H. Hasegawa, M. Tsunoda, F. Matsukura, and H. Ohno, Tunnel magnetoresistance of 604% at 300K by suppression of Ta diffusion in CoFeB／MgO／CoFeB pseudo-spin-valves annealed at high temperature, Applied Physics Letters **93**, 082508 (2008).
[2]   H. Nakayama *et al.*, Spin Hall Magnetoresistance Induced by a Nonequilibrium Proximity Effect, Physical Review Letters **110**, 206601 (2013).
[3]   A. J. Lee, A. S. Ahmed, J. Flores, S. Guo, B. Wang, N. Bagués, D. W. McComb, and F. Yang, Probing the Source of the Interfacial Dzyaloshinskii-Moriya Interaction Responsible for the Topological Hall Effect in Metal/$Tm_3Fe_5O_{12}$ Systems, Physical Review Letters **124**, 107201 (2020).
[4]   J. Fischer *et al.*, Spin Hall magnetoresistance in antiferromagnet/heavy-metal heterostructures, Physical Review B **97**, 014417 (2018).
[5]   J. Fischer, M. Althammer, N. Vlietstra, H. Huebl, S. T. B. Goennenwein, R. Gross, S. Geprägs, and M. Opel, Large Spin Hall Magnetoresistance in Antiferromagnetic $\alpha-Fe_2O_3$/Pt Heterostructures, Physical Review Applied **13**, 014019 (2020).
[6]   G. R. Hoogeboom, A. Aqeel, T. Kuschel, T. T. M. Palstra, and B. J. van Wees, Negative spin Hall magnetoresistance of Pt on the bulk easy-plane antiferromagnet NiO, Applied Physics Letters **111**, 052409 (2017).
[7]   L. Baldrati *et al.*, Full angular dependence of the spin Hall and ordinary magnetoresistance in epitaxial antiferromagnetic NiO(001)/Pt thin films, Physical Review B **98**, 024422 (2018).
[8]   C. O. Avci, K. Garello, A. Ghosh, M. Gabureac, S. F. Alvarado, and P. Gambardella, Unidirectional spin Hall magnetoresistance in ferromagnet/normal metal bilayers, Nature Physics **11**, 570 (2015).
[9]   C. O. Avci, J. Mendil, G. S. D. Beach, and P. Gambardella, Origins of the Unidirectional Spin Hall Magnetoresistance in Metallic Bilayers, Physical Review Letters **121**, 087207 (2018).
[10]   G. Liu *et al.*, Magnonic Unidirectional Spin Hall Magnetoresistance in a Heavy-Metal--Ferromagnetic-Insulator Bilayer, Physical Review Letters **127**, 207206 (2021).

[11]   C. O. Avci, K. Garello, J. Mendil, A. Ghosh, N. Blasakis, M. Gabureac, M. Trassin, M. Fiebig, and P. Gambardella, Magnetoresistance of heavy and light metal/ferromagnet bilayers, Applied Physics Letters **107**, 192405 (2015).

[12]   S. S. L. Zhang and G. Vignale, Theory of unidirectional spin Hall magnetoresistance in heavy-metal/ferromagnetic-metal bilayers, Physical Review B **94**, 140411 (2016).

[13]   Y. Nambu *et al.*, Observation of Magnon Polarization, Physical Review Letters **125**, 027201 (2020).

[14]   A. H. Morrish, Canted Antiferromagnetism: Hematite, (1995).

[15]   Y. Cheng, S. Yu, A. S. Ahmed, M. Zhu, Y. Rao, M. Ghazisaeidi, J. Hwang, and F. Yang, Anisotropic magnetoresistance and nontrivial spin Hall magnetoresistance in Pt/α−Fe_2O_3 bilayers, Physical Review B **100**, 220408 (2019).

[16]   Y. Cheng, S. Yu, M. Zhu, J. Hwang, and F. Yang, Electrical Switching of Tristate Antiferromagnetic Néel Order in α − Fe_2O_3 Epitaxial Films, Physical Review Letters **124**, 027202 (2020).

[17]   T. Fujii, M. Takano, R. Kakano, Y. Isozumi, and Y. Bando, Spin-flip anomalies in epitaxial α-Fe2O3 films by Mössbauer spectroscopy, Journal of Magnetism and Magnetic Materials **135**, 231 (1994).

[18]   S. Gota, M. Gautier-Soyer, and M. Sacchi, Magnetic properties of Fe_2O_3(0001) thin layers studied by soft x-ray linear dichroism, Physical Review B **64**, 224407 (2001).

[19]   C. O. Avci, K. Garello, M. Gabureac, A. Ghosh, A. Fuhrer, S. F. Alvarado, and P. Gambardella, Interplay of spin-orbit torque and thermoelectric effects in ferromagnet/normal-metal bilayers, Physical Review B **90**, 224427 (2014).

[20]   Y. Cheng, E. Cogulu, R. D. Resnick, J. J. Michel, N. N. Statuto, A. D. Kent, and F. Yang, Third harmonic characterization of antiferromagnetic heterostructures, Nature Communications **13**, 3659 (2022).

[21]   Y.-T. Chen, S. Takahashi, H. Nakayama, M. Althammer, S. T. B. Goennenwein, E. Saitoh, and G. E. W. Bauer, Theory of spin Hall magnetoresistance, Physical Review B **87**, 144411 (2013).

[22]   S. Seki, T. Ideue, M. Kubota, Y. Kozuka, R. Takagi, M. Nakamura, Y. Kaneko, M. Kawasaki, and Y. Tokura, Thermal Generation of Spin Current in an Antiferromagnet, Physical Review Letters **115**, 266601 (2015).

[23]   S. J. Williamson and S. Foner, Antiferromagnetic Resonance in Systems with Dzyaloshinsky-Moriya Coupling; Orientation Dependence in αFe2O3, Physical Review **136**, A1102 (1964).

[24]   P. J. Flanders and J. P. Remeika, Magnetic properties of hematite single crystals, The Philosophical Magazine: A Journal of Theoretical Experimental and Applied Physics **11**, 1271 (1965).

[25]   S. Shim, M. Mehraeen, J. Sklenar, J. Oh, J. Gibbons, H. Saglam, A. Hoffmann, S. S. L. Zhang, and N. Mason, Unidirectional Magnetoresistance in Antiferromagnet/Heavy-Metal Bilayers, Physical Review X **12**, 021069 (2022).

[26]   See Section1 of Supplemental Material [url] for Simulation of USMR in Pt/Fe_2O_3, which includes Refs. [27,28].

[27]   K. Ganzhorn *et al.*, Spin Hall magnetoresistance in a canted ferrimagnet, Physical Review B **94**, 094401 (2016).

[28]   H. Wang, Y. Xiao, M. Guo, E. Lee-Wong, G. Q. Yan, R. Cheng, and C. R. Du, Spin Pumping of an Easy-Plane Antiferromagnet Enhanced by Dzyaloshinskii--Moriya Interaction, Physical Review Letters **127**, 117202 (2021).
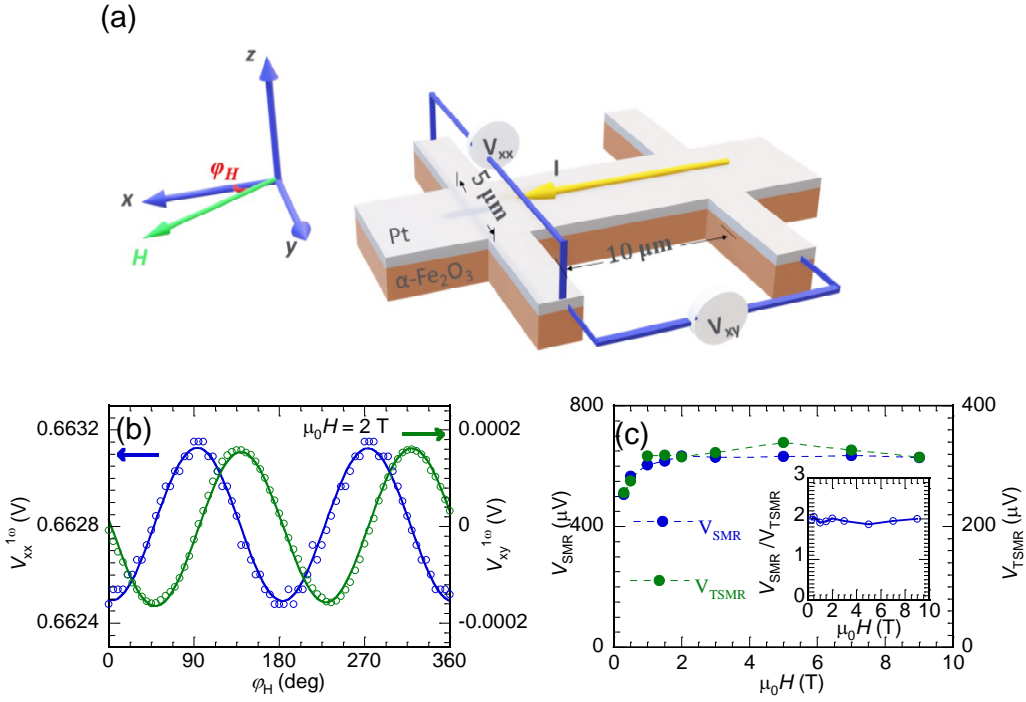
Figure 1. Experimental geometry and first harmonic results. (a) Schematics of a Pt/α-Fe$_2$O$_3$ Hall bar with a 5 µm width and 10 µm length. (b) In plane angular dependence of first harmonic voltage $V_{xx}^{1\omega}$ (blue curve) and $V_{xy}^{1\omega}$ (green curve) for a Pt(5 nm)/α-Fe$_2$O$_3$(30 nm) bilayer at 300 K with 2 T applied field. (c) Field dependence of (transverse) spin Hall magnetoresistance voltage $V_{(T)SMR}$ extracted from the fitting in (b) by Eq. (1) where the inset of (c) shows the ratio of V_{SMR} and V_{TSMR}.
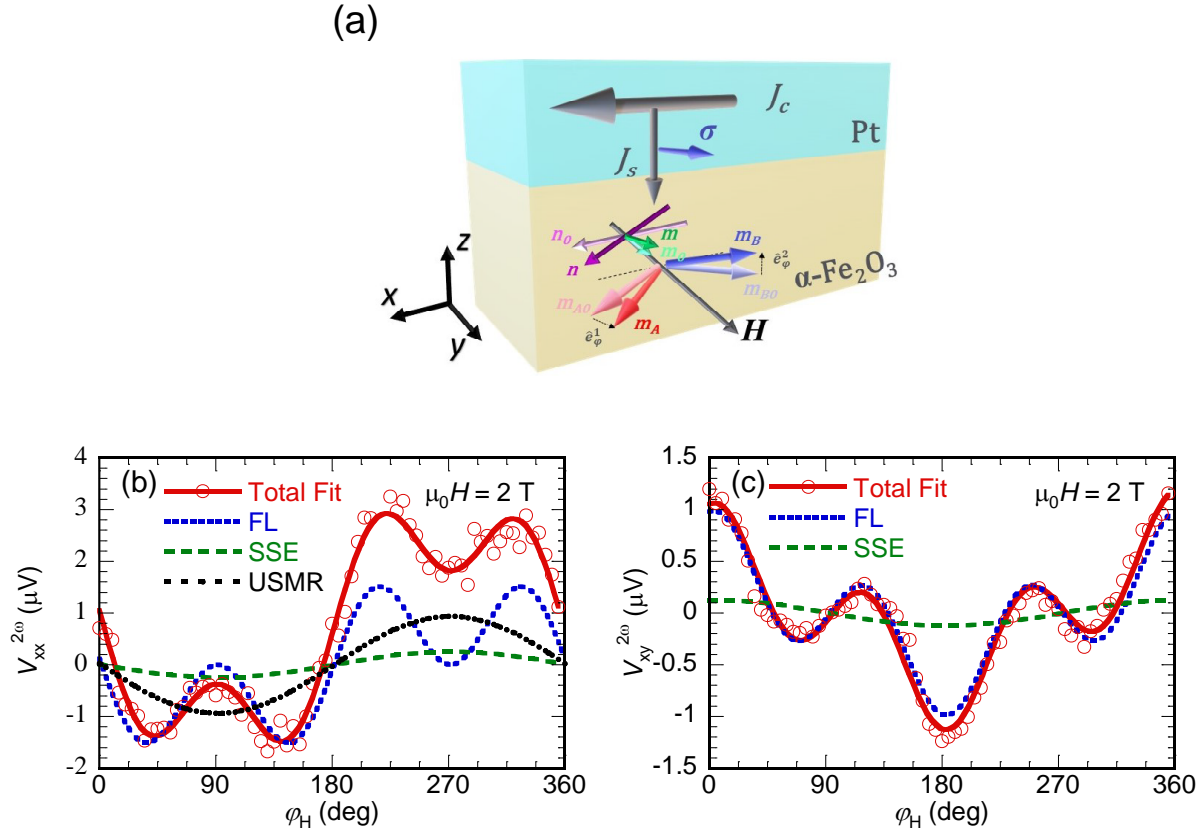
Figure 2. (a) Schematic of current induced spin orbit torque in two spin sublattices $m_{A(B)}$. In-plane angular dependence of second harmonic voltage (b) $V_{xx}^{2\omega}$ and (c) $V_{xy}^{2\omega}$ for the Pt(5 nm)/α-Fe$_2$O$_3$(30 nm) bilayer at 300 K with 2 T applied field. The blue, green and black curves are contributions from the field-like torque, spin Seebeck effect, and USMR, respectively. The red curves are the total fit by Eq. (3) and (4).
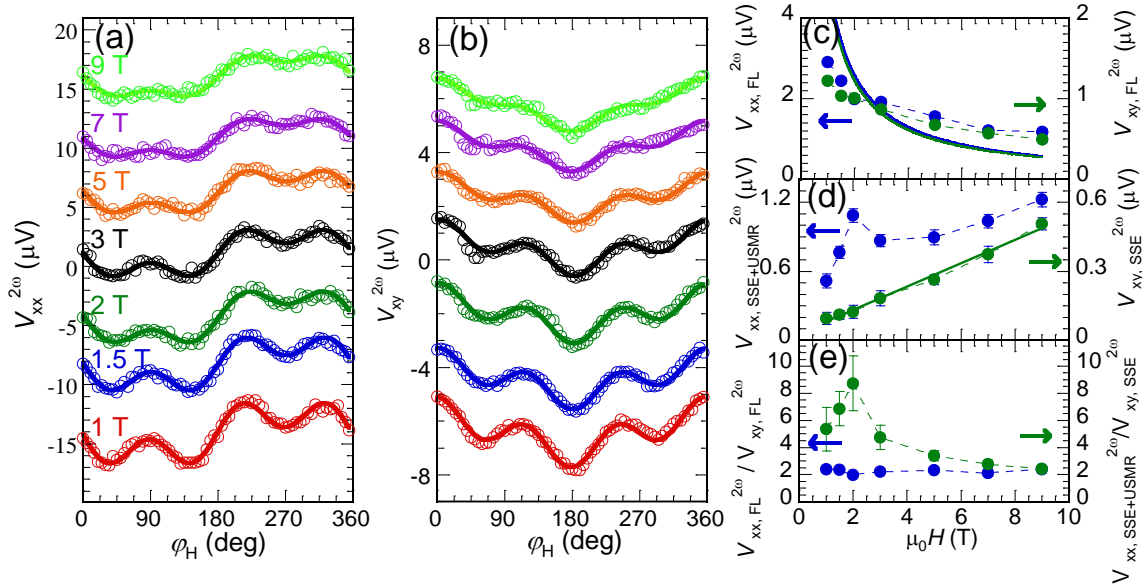
Figure 3. In-plane angular dependence of second harmonic Hall voltage (a) $V_{xx}^{2\omega}$ and (b) $V_{xy}^{2\omega}$ at different magnetic fields for the Pt(5 nm)/α-Fe$_2$O$_3$(30 nm) bilayer at 300 K. (c) Field dependence of field-like torque contribution in $V_{xx}^{2\omega}$ (blue curve) and $V_{xy}^{2\omega}$ (green curve). The solid line is the 1/H fit. (d) Field dependence of spin Seebeck effect contribution in $V_{xx}^{2\omega}$ (blue curve) and $V_{xy}^{2\omega}$ (green curve) . The solid line is the linear fit. (e) The ratio of $V_{xx,FL}$ and $V_{xy,FL}$ (blue curve) and the ratio of $V_{xx,SSE} + V_{xx,USMR}$ and $V_{xy,SSE}$ (green curve), where the magnitude is calculated from (c) and (d). The ratio of $V_{xx,SSE} + V_{xx,USMR}$ and $V_{xy,SSE}$ is greater than 2, which indicates the presence of USMR. Various contributions in (c) to (e) are obtained by fitting like those in Fig. 2.
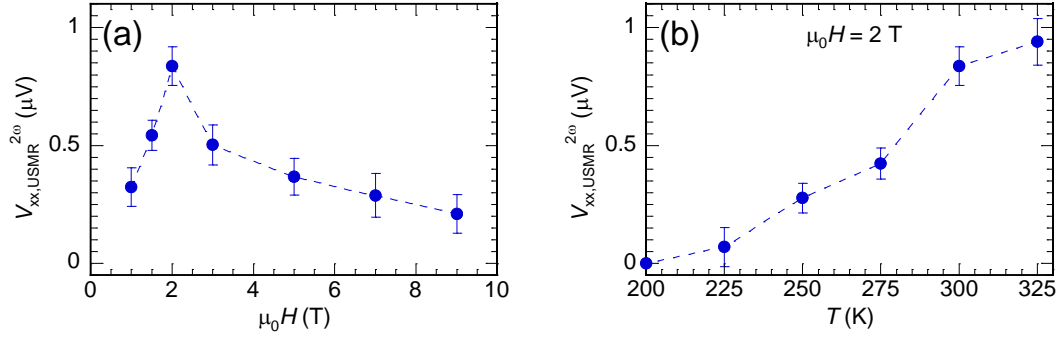
Figure 4. (a) The extracted magnetic field dependence of USMR contribution in the $V_{xx}^{2\omega}$. (b) Temperature dependence of USMR in $V_{xx}^{2\omega}$ at 2 T. The error bars are extracted by the fitting the data in Fig.3.
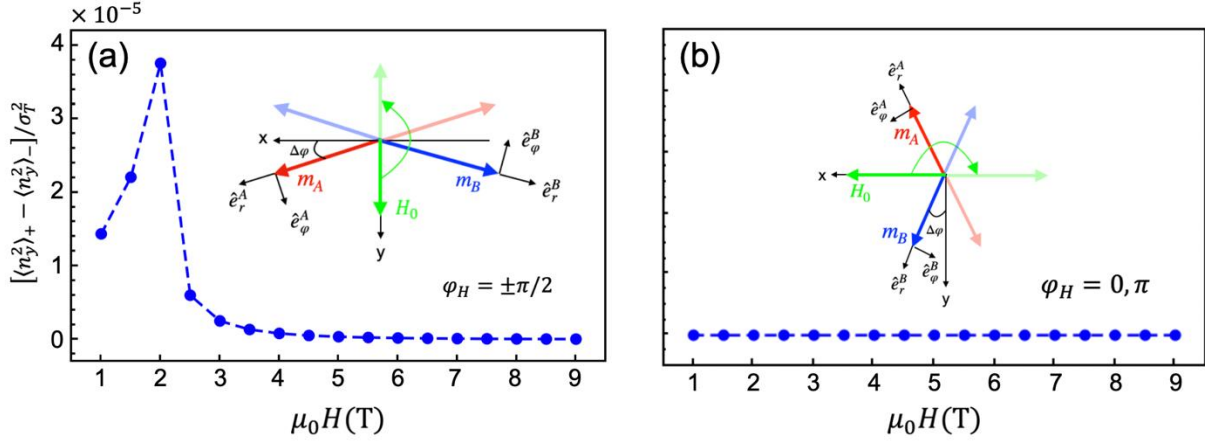
Figure 5. (a) Magnetic field dependence of antiferromagtic magnon number difference between $\varphi_H = \pm\pi/2$ and (b) between $\varphi_H = 0, \pi$. In the insets, the light color arrows (red and blue) represent the sublattice magnetic moments of AFM after rotating $\boldsymbol{H_0}$ (green arrow) to the opposite direction. The magnetic fluctuation originates from the thermal random fields in the two orthogonal $\hat{e}_\varphi$ and $\hat{e}_r$ directions. σ_T^2 is the thermal coefficient.